Experimental Demonstration of Dynamic Focusing of a Relativistic Electron Bunch by an Overdense Plasma Lens

G. Hairapetian, P. Davis, C. E. Clayton, and C. Joshi
Department of Electrical Engineering, University of California at Los Angeles, Los Angeles, California 90024

S. C. Hartman and C. Pellegrini
Department of Physics, University of California at Los Angeles, Los Angeles, California 90024

T. Katsouleas
Department of Electrical Engineering, University of Southern California, Los Angeles, California 90089
(Received 19 November 1993)

Dynamic focusing of a 3.8 MeV electron bunch, a few collisionless skin depths long $\sim 3c/\omega_p$, by an overdense, thick plasma lens has been demonstrated. Because of electron inertial effects, the head of the bunch is virtually unaffected by the lens while the rest is focused to varying degree. Time-resolved measurements performed 31 cm downstream of the plasma lens show that, in time, the bunch pinches from an initial size of 2.7 mm (FWHM) to about 0.57 mm and then expands, in reasonable agreement with theory.

PACS numbers: 52.40.Mj, 41.75.Ht

In recent years, there has been a growing interest in the accelerator physics community to explore plasma based lenses [1] and accelerators [2]. In principle, a plasma lens can provide an azimuthally symmetric, focusing gradient of ~ 100 MG/cm, exceeding that of conventional quadrupole lens by several orders of magnitude [3]. Increasing the focusing gradients of conventional lenses is one of the main challenges for the future colliders where beams of extremely small spot sizes and high luminosity are required at the interaction point [4]. However, because the colliding bunches [4,5] in these machines are short (< 10 ps) and nonuniform in time, the focusing process would be highly dynamic if a plasma lens is utilized. In this Letter, such dynamic focusing of a 3.8 MeV, 25 ps (FWHM) long electron bunch by an overdense plasma lens ($n_b \ll n_p$ where n_b and n_p are the bunch and plasma density, respectively) has been demonstrated for the first time.

The basic concept of a plasma lens is as follows [6]: As a relativistic electron beam enters a plasma, the plasma electrons charge neutralize the beam on a $1/\omega_p$ time scale, where ω_p is the plasma electron frequency. However, if the collisionless skin depth (c/ω_p) is larger than the beam radius, most of the axial plasma return current flows on the outside of the beam, and the beam current is not fully neutralized. Consequently, the beam pinches [7] radially due to its own magnetic field. This is in contrast to the "active" plasma lens [8] (e.g., a z-pinch plasma) where the focusing magnetic field is due to an externally driven plasma current. Experimentally, relativistic electron beam self-focusing and guiding in plasmas have been observed [9]. In most of these experiments, however, the plasma length was much longer than the betatron oscillation wavelength [$\lambda_\beta = 2\pi r_0/(2I/I_A)^{1/2}$ where r_0 is the beam radius, and I and I_A are the beam and Alfvén currents, respectively]. As a result, the beam undergoes multiple, large amplitude, transverse oscillations which lead to transverse emittance growth [10]. Eventually, the betatron oscillations are damped due to a spread in the betatron wavelength [11] (phase mixing), and the beam attains an equilibrium radius which has been previously measured [9,12]. For the plasma lens to be useful, the plasma column, must be shorter than $\lambda_\beta/4$ to prevent the degradation of the beam emittance which ultimately limits the minimum spot size. In this experiment, the focal length of the plasma lens was longer than the length of the plasma column. In analogy to an optical lens, the plasma lens imparts a radially symmetric, inward kick to the azimuthally symmetric bunch which brings it to a focus outside of the plasma. The only other reported plasma lens experiment [13] has demonstrated a very limited focusing, less than a 20% reduction in spot size, and with no temporal resolution. In this Letter, we report the results of an experiment where the dynamic focusing process, which leads to a factor of 4 reduction in transverse bunch size, is time resolved.

The experiment was performed with a laser driven, photocathode RF accelerator [14] which produces 25 ps long, 3.8 MeV electron bunches at 1 Hz containing up to 1.5 nC per bunch. The electron bunches were transported to the plasma chamber located 2 m downstream of the gun with a focusing solenoid at the exit of the accelerator and four steering magnets along the beam line. The plasma chamber which was filled with Ar gas up to a pressure of 20 mTorr was connected to the RF gun ($p < 5 \times 10^{-8}$ Torr) through a windowless, two stage differential pumping system. Each pumping stage consisted of a low conductance tube followed by a turbomolecular pump. Since the beam encountered no windows, the beam emittance was not degraded due to multiple scattering. The plasma

0031-9007/94/72(15)/2403(4)$06.00

($n_p \leq 6\times10^{12}$ cm^{-3}, $kT_e \approx 2$ eV) was produced by an RF discharge in a glass tube (diam of 1.7 cm, length of 12 cm). The RF amplifier (10–20 MHz, 800 W) was connected via a capacitive tuning circuit to a helical antenna (5.5 cm long, 12 turns) wrapped on the outside of the glass tube. The pulsed ($t_{on}=5$ ms, $t_{off}=195$ ms) plasma was diagnosed by a small cylindrical (diam of 0.76 mm, length of 2.5 mm) Langmuir probe which was calibrated against a 62.5 GHz microwave interferometer. The shot-to-shot fluctuations of the plasma density were measured to be less than 5%. The axial plasma density profile was also determined independently by measuring the emission intensity profile of the Ar^+ (480 nm) line, details of which will be published elsewhere. The plasma which was not confined by an external magnetic field had a flat-top (0.8 cm) radial profile, and a bell-shaped axial profile ($\Delta z=7.5$ cm FWHM). The plasma was collisionless ($\omega_p \gg \nu_{en}$ and $\tau_b \nu_{en} \approx 0.01$, where ν_{en} is the plasma electron-neutral collision frequency [15] and τ_b is the bunch length). Therefore, the plasma return currents were not influenced by the plasma electron-neutral collisions. Because of the short bunch length, the effects of neutral gas on the beam electrons were also negligible ($\nu_{ion} \ll 1/\tau_b$, where ν_{ion} is the collisional ionization frequency [16]).

The electron bunch was characterized with a variety of diagnostics [Fig. 1(a)] which include the following: four retractable, linear phosphor-coated screens (PS 1 to 4) both upstream and downstream of the plasma chamber for spot size measurements, three retractable Faraday cups (not shown), a current transformer (not shown) for nondestructive measurement of beam charge, and a Cherenkov radiator (CR) downstream of the plasma for time-resolved spot size measurements. The electron bunch, which initially contained up to 1.5 nC of charge, was scraped by the two low conductance tubes. Up to 0.6 nC ($I_{peak} \leq 20$ A) was transported to the plasma chamber as independently measured by the Faraday cups and the current transformer. Because of the low energy ($\gamma=7.5$) and the high charge ($Q \leq 0.6$ nC) of the bunch, the bunch transport was space charge dominated [0.2 < (emittance force)/(space charge force) < 1.3]. To estimate the bunch emittance, the transverse bunch size was measured at four axial positions (PS1–PS4) for different bunch currents ($I \approx 2$ to 20 A). With the emittance as the fit parameter, the measured transverse beam sizes are fitted by the solution of the beam envelope [17] equation with space charge. A normalized emittance of about 10π mm mrad gives the best fit (within 10% of data), which agrees very closely with PARMELA simulations. At the entrance of the plasma lens, the bunch has a transverse time-integrated dimension of 2.3 mm FWHM and is radially expanding; i.e., the bunch is not at a waist. The transverse bunch profile can be approximated roughly as a Gaussian ($\sigma_r \approx 1$ mm and $n_b < 5\times10^{10}$ cm$^{-3} \ll n_p$). Since $k_p\sigma_r < 0.4$ where k_p is ω_p/c, most of the plasma return current [18,19] flows on the outside of the beam, and the beam magnetic field is not fully neutralized.

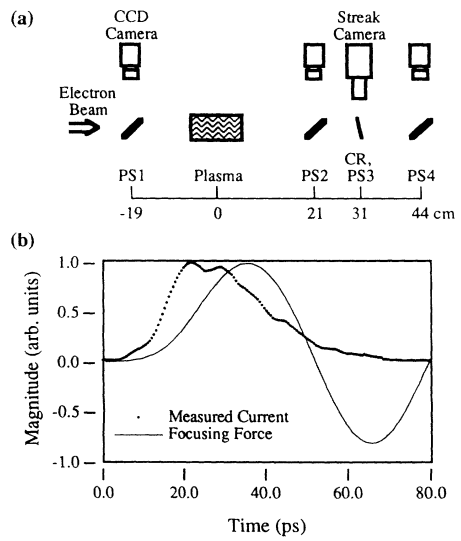

FIG. 1. (a) Schematic drawing of the experimental setup, and the axial positions of the phosphor screens (PS1–PS4) and the Cherenkov radiator (CR). (b) Measured temporal profile (normalized) of the electron bunch, and the calculated profile (normalized) of the focusing force for $n_p=4\times10^{12}$ cm^{-3}.

Space- and time-resolved profiles of the bunch are obtained by streaking the Cherenkov light from a 500 μm thick fused-silica radiator which is mounted on a retractable shaft 31 cm downstream of the plasma lens. The temporal resolution of the combined streak camera and the Cherenkov radiator system is less than 5 ps FWHM. The Cherenkov radiation generated when the beam traverses the radiator is imaged onto the 100 μm vertical slit of the camera yielding a vertical resolution of 33 μm. Figure 1(b) shows the normalized temporal profile of the beam in the absence of the plasma. Using this measured temporal beam profile, the exact temporal profile of the focusing force can be calculated from the plasma wake-field solutions [5,18] which incorporate electron inertia and plasma return currents. A typical profile of the calculated transverse wake field for $n_p=4\times10^{12}$ cm^{-3} is shown in Fig. 1(b). At the head of the bunch (~ first $1/\omega_p$), the focusing force is essentially zero. The focusing force increases in time and reaches its maximum near the tail. Figure 2(a) shows the streaked image of a vertical slice through the center of the beam in the presence of the plasma. For analysis, the streaked image is divided into 5 ps wide (resolution of camera) vertical strips. Each strip is integrated in time to obtain the vertical beam dimension (FWHM) which are then plotted versus time along with the peak intensity in Fig. 2(b). As predicted, the head of the beam is virtually unaffected by the plasma. In approximately 20 ps, the beam focuses from about 2.7 mm to 0.57 mm. Consequently, the peak intensity increases by a factor of 13 (saturation effects in the

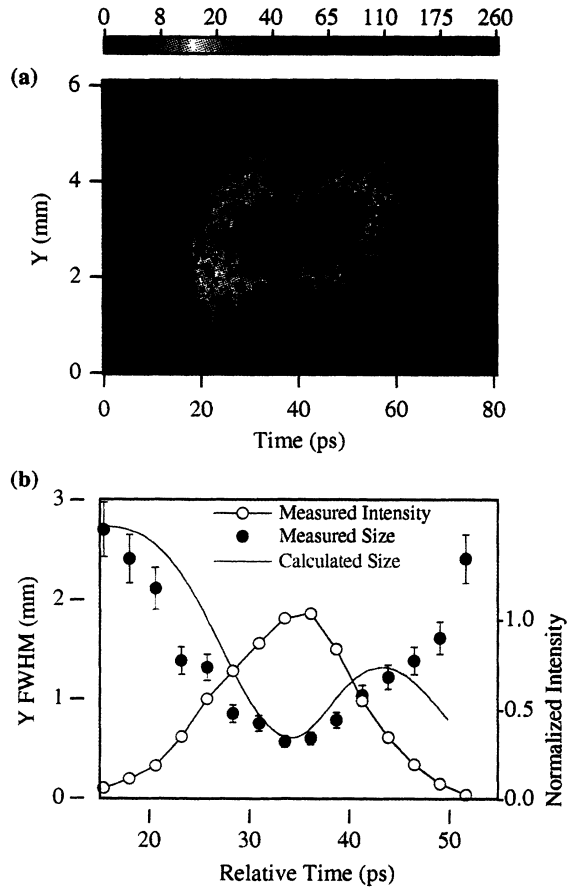

FIG. 2. (a) The streak image of the bunch taken 31 cm downstream of the plasma. (b) The FWHM and normalized peak intensity of the bunch as a function of time extracted from the streak image (points). The calculated temporal profile is also plotted in red.

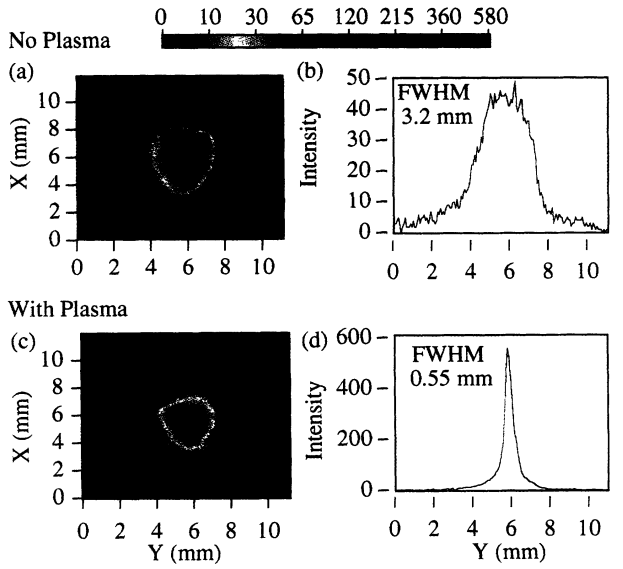

FIG. 3. (a) Time-integrated bunch image with no plasma taken 21 cm downstream of the plasma. (b) A vertical lineout of the image in (a). (c) Time-integrated bunch image in the presence of the plasma. (d) A vertical lineout of the image in (c).

streak camera reduce the measured peak intensity by about 20%). At later times, the beam is overfocused as the focusing force increases. Since the lens has a time-dependent focusing force, the focal length of the lens is not unique. Different axial parts of the beam come to a focus at different axial positions. This nonuniform focusing gives rise to longitudinal abberations which would limit the increase in the bunch luminosity [6] in a collider.

Neglecting chromatic and spherical abberations, one can use a paraxial beam approximation to numerically estimate the average transverse beam size as a function of axial position. The electron bunch is divided into eleven, evenly spaced, infinitesimally thin slices in time, and the envelope equation [17] is solved for each slice. Since the plasma density and the bunch profiles were measured in detail, the focusing force for each slice in time can be numerically calculated from the transverse wake-field [5,18] solutions as a function of plasma density profile. Our model assumes a self-similar transverse profile, and it ignores any variations in the initial transverse bunch size and the angular divergence along the bunch. For comparison purposes, the calculated transverse bunch profile in time at the position of the Cherenkov radiator is shown in Fig. 2(b). Considering the simplicity of our model which also ignores azimuthal asymmetries, the calculated and measured bunch sizes agree quite reasonably at earlier times and at the best focus, but deviate at later times.

The focusing is so robust that even the time-integrated beam images on the phosphor screen clearly show the focusing. With no plasma, Figs. 3(a) and 3(b) show the time-integrated beam size at PS2. The vertical dimension of the unfocused beam is about 3.2 mm FWHM. When the plasma is turned on, the beam is observed to focus down to about 0.55 mm [Figs. 3(c) and 3(d)]. The spatially integrated intensity of the image which is proportional to the total charge is conserved. In addition, independent charge measurements confirm that all (to within 5%) of the beam charge upstream of the plasma is transported to the end of the beam line. The beam spot size increases to about 1.0 mm FWHM at PS3. This compares well with the time-integrated, streaked image (1.1 mm FWHM) from the Cherenkov radiator measured at the same axial position. At PS4, the transverse beam size increases to about 1.1 mm FWHM (Fig. 4). The time-dependent bunch sizes calculated from the model discussed earlier can be combined to obtain the predicted time-integrated transverse bunch profiles [20]. The calculated results which are plotted in Fig. 4 agree

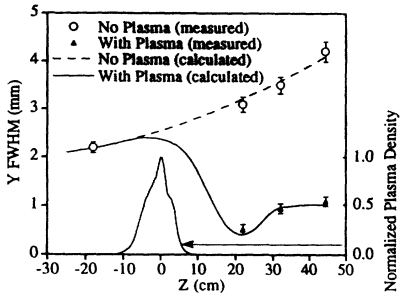

FIG. 4. Time-integrated transverse bunch sizes (FWHM), measured and numerically calculated, as a function of axial position along with the normalized axial profile of the plasma density.

quite well with the experimental measurements. In addition, Fig. 4 indicates that the best focus occurs near PS2. The small discrepancy between the measured spot size of 0.55 mm and the calculated value of 0.47 mm at the best focus, could be due to spherical abberations which in theory limit the final spot size to about $\frac{1}{4}$ of the initial size [6] for a Gaussian profile. It is also worth noting that the time-resolved measurements were not performed at the best focus where a time-resolved spot size of 0.37 mm is predicted. Another interesting feature is that the beam envelope is not symmetric about the best focus as confirmed by the measurements. This is a direct result of time-dependent focusing. Since the integrated transverse beam size (FWHM) is mainly determined by the focused (highest intensity) part of the beam, as different parts of the beam come to a focus at different axial positions it appears as though the beam stays focused over a longer axial distance.

In summary, we have investigated the focusing properties of an overdense ($n_b \ll n_p$), thick plasma lens. Time-resolved measurements of the focused bunch indicate that the head of the beam, the first $1/\omega_p$, is not focused and the tail is overfocused as predicted by the theory. The time-integrated measurements of the spot size downstream of the plasma lens are in good agreement with the results of the numerical model. A full particle-in-cell simulation of the experiment is underway and will be reported elsewhere.

The authors acknowledge helpful discussions with K. Marsh, J. B. Rosenzweig, J. J. Su, and H. Zwi. Also, expert technical assistance from N. Barov, M. Fauver, M. Hogan, P. Kwok, S. Park, G. Travish, and R. Zhang is greatly appreciated. This work is supported by SDIO/IST through ONR Grant No. N00014-90-J-1952 and U.S. DOE Grants No. DE-FG03-92ER-40727, No. DE-FG03-92ER-40493, and No. DE-FG03-92ER-40745.

[1] P. Chen, Part. Accel. **20**, 171 (1987).
[2] J. M. Dawson, Sci. Am. **260**, 54 (1989).
[3] T. Katsouleas *et al.*, Phys. Fluids B **2**, 1384 (1990).
[4] B. Richter, IEEE Trans. Nucl. Sci. **32**, 8 (1985).
[5] P. Chen *et al.*, IEEE Trans. Plasma Sci. **15**, 218 (1987).
[6] J. J. Su *et al.*, Phys. Rev. A **41**, 3321 (1990).
[7] W. H. Bennett, Phys. Rev. **45**, 890 (1934).
[8] E. Boggasch *et al.*, Phys. Rev. Lett. **66**, 1705 (1991).
[9] S. E. Graybill and S. V. Nablo, Appl. Phys. Lett. **8**, 18 (1966); W. E. Martin *et al.*, Phys. Rev. Lett. **54**, 685 (1985).
[10] S. Humphries, Jr., *Charged Particle Beams* (J. Wiley and Sons, New York, 1990), p. 159.
[11] J. J. Su *et al.*, IEEE Trans. Plasma Sci. **15**, 192 (1987).
[12] J. B. Rosenzwieg *et al.*, Phys. Fluids B **2**, 1376 (1990).
[13] H. Nakanishi *et al.*, Phys. Rev. Lett. **66**, 1870 (1991).
[14] C. Pellegrini *et al.*, in 1993 Proceedings of Particle Accelerator Conference (to be published).
[15] S. C. Brown, *Basic Data of Plasma Physics* (MIT Press, Cambridge, MA, 1966).
[16] F. F. Foster and W. Prepejchal, Phys. Rev. A **6**, 1507 (1972).
[17] Humphries, Jr., (Ref. [10]), p. 211.
[18] J. L. Cox, Jr. and W. H. Bennett, Phys. Fluids **13**, 182 (1970).
[19] R. Keinings and M. E. Jones, Phys. Fluids **30**, 252 (1987).
[20] At each axial position, the transverse bunch sizes are integrated in time by assuming a Gaussian profile and summing the calculated beam sizes (FWHM) with a weighting factor proportional with the current and inversely proportional to the beam size squared. This process is repeated at several axial position to obtain the time-integrated beam envelope trace.

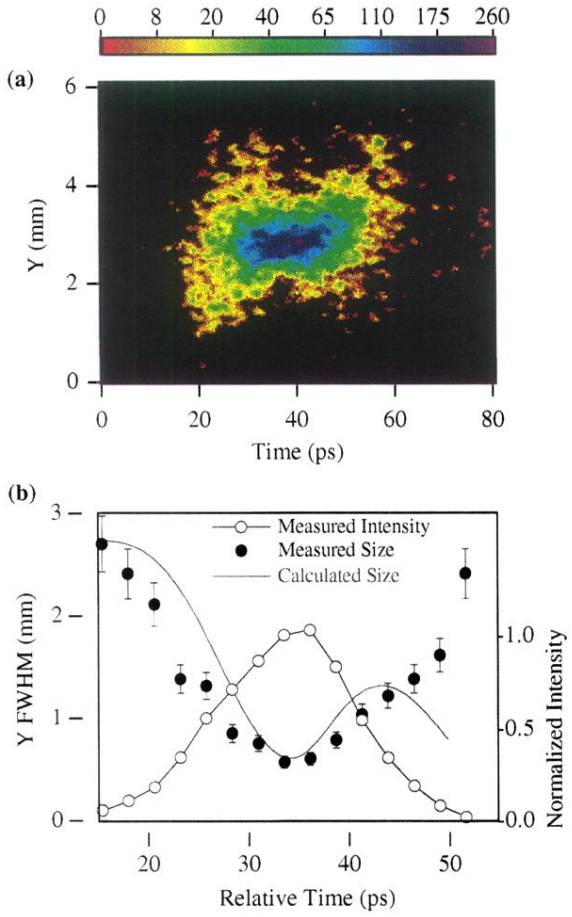

FIG. 2. (a) The streak image of the bunch taken 31 cm downstream of the plasma. (b) The FWHM and normalized peak intensity of the bunch as a function of time extracted from the streak image (points). The calculated temporal profile is also plotted in red.

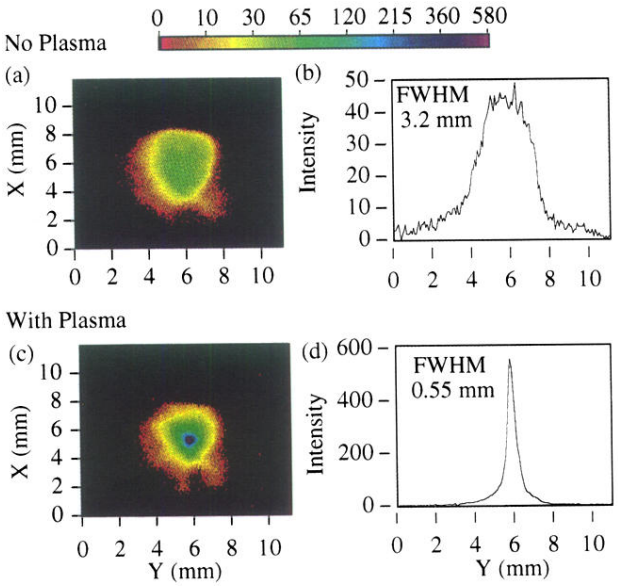

FIG. 3. (a) Time-integrated bunch image with no plasma taken 21 cm downstream of the plasma. (b) A vertical lineout of the image in (a). (c) Time-integrated bunch image in the presence of the plasma. (d) A vertical lineout of the image in (c).